Improved design of a high lift system for general aviation aircraft

Florjancic, D.; Steenhuizen, D.; Veldhuis, L. L M

Publication date
2016

Document Version
Final published version

Published in
30th Congress of the International Council of the Aeronautical Sciences, ICAS 2016

ICAS 2016
30th Congress of the International Council of the Aeronautical Sciences
DCC, Daejeon, Korea ; September 25-30, 2016

IMPROVED DESIGN OF A HIGH LIFT SYSTEM FOR GENERAL AVIATION AIRCRAFT

D. Florjancic, D. Steenhuizen, L.L.M. Veldhuis
Delft University of Technology, Delft, The Netherlands

Keywords: *high lift devices, aerodynamic design, optimization*

Abstract

Optimization of a single slotted flap with dropped hinge is performed with the objective of increasing the payload of a propeller driven 4-seater general aviation aircraft. Within the optimization loop, two-dimensional aerodynamic characteristics are evaluated using the MSES code, while three-dimensional aerodynamic characteristics and weight are estimated with semi-empirical methods. Genetic and pattern search algorithms are used to minimize the objective function. It is found that the payload can be increased by up to 40% if the stall speed is kept constant. Cruise drag due to flap support fairings increases the fuel burn for 3% on a range of 1000 nm. A method of using the maximum displacement thickness on the flap trailing edge in order to detect separation during optimization is proposed and found to be reliable.

1 Introduction

Modern general aviation aircraft designs tend to have relatively high wing loading in order to decrease aircraft empty weight and fuel burn for the same payload as described in reference [12]. The benefits of higher wing loading come at the expense of low-speed performance. Higher lift coefficients are needed to carry the same weight at the same dynamic pressure on a smaller wing. The main function of high lift systems is to provide higher lift coefficient in take-off and landing configurations, while affecting the cruise performance as little as possible.
An exemplary modern 4-seater propeller driven aircraft is employed with a plain flap high lift system. The improvement of this system is the subject of the project. The initial objective is:

Design an improved high lift system that can replace the current plain flap system with no or very little changes to the existing wing structure. The aerodynamic shape of the wing in cruise condition may not change. The goal of the improved high lift system is to increase the payload by keeping the stall speed with full flaps the same. Cruise speed and range should also stay the same. The effect on field performance should be identified.

The research question is formulated as follows:

What is the optimal high lift system design for a highly efficient 4-seater general aviation aircraft for improved payload?

Figure 1 shows the wing planform and airfoil cross section in clean configuration with plain flap installed. The newly designed flap must preserve the same clean configuration aerodynamic shape, may not extend further than the rear spar position (approximately at 0.7c) and must keep the same span and spanwise position.
A preliminary performance analysis was first performed that assumed an increase in lift coefficient by up to 0.25. Increased drag due to flap mechanism fairings and increased aircraft empty weight due to higher MTOW were estimated. The results of this study suggested that the increase in maximum lift coefficient is the most important aspect of increasing the payload. From consideration of available data in open literature (references [9], [7], [2]) and analysis of existing high lift systems on general aviation aircraft it was decided that the most

appropriate type of high lift system to meet the project objectives is a single slotted flap with dropped hinge mechanism. Two-dimensional aerodynamic optimization of a single slotted flap therefore presented the core activity of the design process. Within the optimization, three dimensional aerodynamic characteristics were estimated using semi-empirical methods. Impact of increased wing, landing gear and fuel weights was also estimated using semi-empirical models and performance calculation.

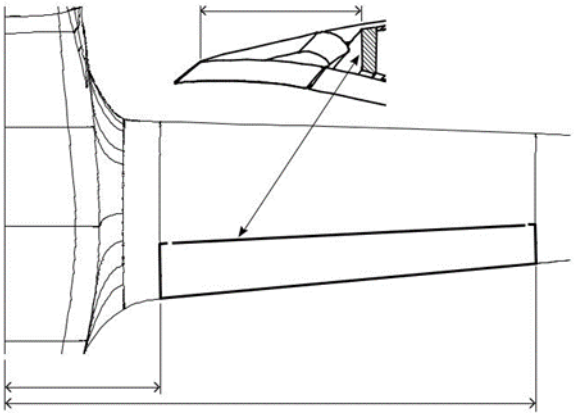

Fig. 1: Existing wing planform and airfoil section with plain flap.

2 Methodology

2.1 Performance model

In order to evaluate the effect of the improved high lift system on the aircraft's overall performance, a model is established to calculate the take-off and landing distance and fuel weight for given range. Equations from reference [11] are used to calculate the performance parameters after the aerodynamic characteristics and empty weight are established.

2.2 Two-dimensional aerodynamic analysis and design

The MSES code, described in reference [8], was chosen as the tool for airfoil analysis and design. It is an established open source code that couples Euler equations for inviscid flow with

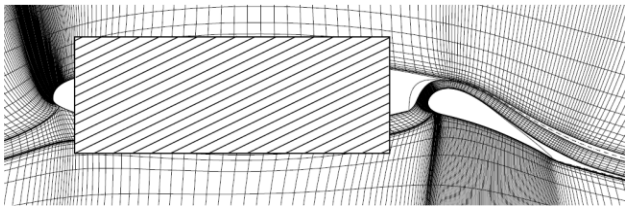

Fig. 2: MSES grid about a two-element airfoil section.(part of the figure masked because of confidentiality reasons)

boundary layer equations into a single non-linear system of equations that is solved by a Newton-Raphson iterative method. MSES is capable of analyzing multi-element airfoils that are the main subject of this project. A typical MSES grid is shown in figure 2. Grid generation is done automatically by placing the streamwise grid lines on the precomputed inviscid flow streamlines and intersecting them with vertical grid lines emitting from the airfoil surface on user specified number of points.
Flap geometry for each design case was constructed within a number of constraints. In retracted position, the clean airfoil had to be unchanged. For reference clean configuration, the airfoil at approximately the midspan of the flap was chosen. At stall speed and sea level the Reynolds number for this airfoil is 2.1×10^6 and Mach number is 0.09. These two conditions were also used in MSES analysis. Any deployed position of the flap had to be consistent with a fixed hinge position, as it was assumed that a simple dropped hinge mechanism will be used to deploy the flap. Design variables in the design of the flap were therefore the chordwise positions of the upper and lower surface flap breaks - the forward most points of the flap that are wetted in the stowed configuration (*C1*, *C2*), the hinge point position (HP_X , HP_Y), the flap angle (f), and the position of the additional four control points that define the b-spline that forms the part of the flap stowed in the cove in clean configuration. Design variables are indicated in figure 3. The main element edges at flap breaks were kept sharp to enclose the flap in clean configuration. At the bottom edge this inevitably causes separation, but MSES can handle such flow by assuming a closed separation bubble inside the separation region. The cove shape used in

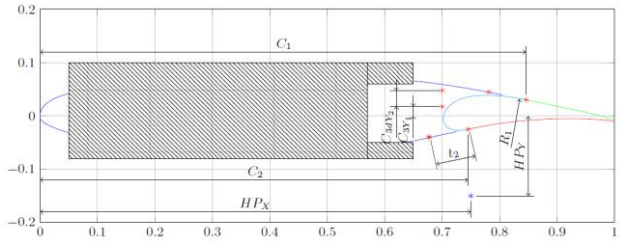

Fig. 3: Exemplary flap defined by clean airfoil and a b-spline with 6 control points. The point in blue is the hinge point. (part of the figure masked because of confidentiality reasons)

MSES calculations was simplified as shown in figure 4 by the black curve. In figure 3 a portion of the b-spline defining the flap is still wetted by the flow in clean configuration, because it was taken into account that the main element trailing edges have finite material thickness, which was set to 0.002c. This represents a minimum thickness of 1.8 mm at the flap outboard edge. Generation of flap geometry in retracted and deployed configuration was automated using MatLab. MSES grid generation and solver settings were automated using Linux scripts. Optimization routine is explained in subsection 2.8

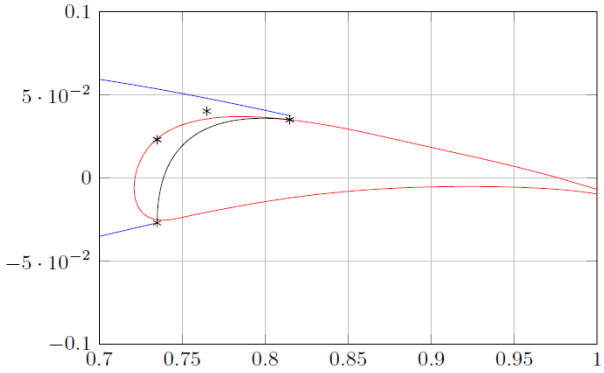

Fig. 4: Simplified cove shape for MSES runs.

2.3 Estimation of three-dimensional aerodynamic characteristics

Empirical estimation methods were used for predicting three-dimensional characteristics of the whole aircraft based on flight test data for the clean configuration (flaps retracted) and on two-dimensional airfoil data for deployed flaps. ESDU 91014 [3] was used to estimate the maximum lift coefficient of a finite wing. The method is based on statistical data of various designs and uses the following parameters to determine the increase in maximum lift coefficient due to deployed flaps: wing planform, flap span and increase in two-dimensional lift coefficient as compared to the clean airfoil. It also uses correction factors for Reynolds number and type of flaps. When data is obtained for a particular wing, the method only uses a single equation to determine the lift coefficient increment depending on the two dimensional lift coefficient of the flapped airfoil. Equation (1) was used for the present wing.

$$\Delta C_{L\,max,3D} = \Delta C_{l\,max,2D} \cdot 0.486 \qquad (1)$$

The only variable in equation (1) is $C_{l\,max,2D}$ that is the diff erence in $C_{l\,max,2D}$ computed by MSES and clean airfoil $C_{l\,max,2D}$. Aforementioned method does not take into account the angle of attack at which the $C_{l\,max}$ is found, but all designs are evaluated at the same angle of attack in MSES. Although the method may not return the most accurate three dimensional lift coefficient, it is sufficient for the comparison and grading of similar designs.
Induced drag is estimated by the method from reference [18] that uses equation (2) where K_{Cdi} is a correction factor based on flap span, wing aspect ratio and flap cut-out.

$$C_{Di} = \frac{C_L^{\,2}}{\pi A e}\left(1 + K_{C_{Di}}\left(\frac{\Delta C_L}{C_L}\right)^2\right) \qquad (2)$$

Finite wing profile drag for a given angle of attack is calculated from two-dimensional profile drag coefficients for each spanwise station at a given angle of attack (equation (3)).

$$C_{Dp} = \int_0^{b/2} C_D(y)\frac{c(y)}{c_{ref}}\,dy \qquad (3)$$

For simplicity, the drag polars for only three spanwise stations along the wing were obtained to form a database for profile drag computation. For analysis of take-off performance (not used within the optimization loop, only for final design) when aircraft is operating at maximum L/D instead of maximum C_L, a method to predict $C_{L,3D}$ at any angle of attack is needed.

ESDU 93019 [4], a method to predict lift increment of wings due to flaps at zero angle of attack, was applied also to higher angles of attack after it was correlated with the VSAERO code (described in subsection 2.7) and found to give reasonable agreement.
Equation 4 is used where a_1 is the lift curve slope of the clean wing at zero angle of attack and $K_{\Delta CL}$ is a correction factor based on wing planform and spanwise location of flaps.

$$\Delta C_{L3D} = \Delta C_{l2D} \cdot \frac{a_1}{2\pi} \cdot K_{\Delta C_L} \qquad (4)$$

2.4 Flap and mechanism bracket sizing

Flap weight estimation was excluded from the optimization loop due to following reasons. The dimensions of the slotted flap are comparable to the plain flap currently in use. The maximum load on the flap in retracted configuration is comparable to the maximum loading on the flap in clean configuration, mainly because FAR 23 [1] dictates that the aircraft should be sized to withstand a load factor of 2.2 with flaps deployed and 4.4 when retracted. The mass of the plain flaps presently in use is also negligible compared to the expected increase in MTOW during optimization process.
Dropped hinge mechanism requires three brackets per flap sticking out of the bottom surface of the wing. Since the aircraft in the present configuration with plain flap does not possess any such external fairings, the drag of dropped hinge mechanism fairings in cruise configuration should be taken into account and computed within the design optimization loop. It was assumed that the fairing is shaped as an airfoil with blunt trailing-edge. Emperical data from chapter 3 of reference [10] was used to estimate this drag.

2.5 Drag of mechanism fairings

Contrary to the flap itself, dropped hinge mechanism brackets represent additional parts for the implementation of slotted flaps, therefore they are sized within the optimization scheme. Actuation torque is calculated for each iteration in the optimization scheme. Although for the optimized flaps the torque is found to be up to two times larger than for the plain flap, the actuator weight increases from about 2 kg to about 3 kg according to data available in reference [13]. Therefore the change in actuator weight was decided to be negligible compared to the increase in payload and was not accounted for in the optimization loop.

2.6 Wing and landing gear weight estimation

Weight of both the wing and the landing gear increases due to increase in *MTOW* during the optimization. Those weights are not negligible and are therefore estimated. Wing weight is estimated with the model proposed by reference [16]. When the required data for the aircraft is used, the wing weight is proportional to the *MTOW*, see equation (5).

$$W_{wing} = MTOW \cdot 0.0864 \qquad (5)$$

For landing gear weight prediction the model from reference [15] is used. It is based on statistical data and separately determines the weight of the nose and main landing gear. Equation (6) is used where coefficients *A*, *B*, *C* and *D* are determined based on aircraft and landing gear type.

$$m_{nose\,gear} = A + B \cdot MTOW^{4/3} + C \cdot MTOW + D \cdot MTOW^{3/2} \qquad (6)$$

2.7 Three dimensional aerodynamic analysis with VSAERO

To correlate the semi-empirical estimation methods and to estimate the drag coefficient of air-craft's fuselage and landing gear based on comparison of computed wing-only polars with flight test results, the VSAERO code was used. It is a potential flow panel code coupled with boundary layer method. User needs to discretize the geometry with panels and prescribe wake panels to represent vorticity in the wake. VSAERO performs iterative calculation during which the wake shape is changing until

convergence (figure 6). After wake iterations, inviscid-viscous iterations are performed to calculate the boundary layer characteristics and corrected inviscid pressure distributions over the wing, while wake geometry stays constant. VSAERO can detect boundary layer separation, but does not alter the calculation according to the separated flow since the separation is always assumed where the user prescribes the wakes. It is possible to change the wake separation position to the detected boundary layer separation and run the calculation again, but the process is time consuming and it is difficult to judge its accuracy. In case of flap designs that were the subject of this project, the lift limiting phenomena at high angles of attack was not boundary layer separation off the surface but rather wake bursting, which is impossible to account for in VSAERO. It is therefore expected that VSAERO over-predicts $C_{L,max3D}$, but can still be used for lift, drag and pitching moment calculations at lower angles of attack.

2.8 Optimization scheme

A combination of global and local optimization algorithms was used to find the optimum flap design. The problem of optimizing the flap geometry is highly global. For example, the same gap and overlap of the flap can be obtained with different combinations of flap geometry, hinge position and deployment angle. Global optimization algorithm is therefore necessary, but in general it takes too long to finish. During initial runs of MatLab's genetic algorithm it was noted that the decrease in objective function was levelling out after 10 to 20 generations and only offered small improvements for a lot of additional computation time. Therefore the global optimization was terminated when a clear pattern emerged and the best design was used as a starting point for local optimization performed with MatLab's pattern search algorithm. At every stage of optimization some designs emerged that had no convergence in MSES runs, which is why a gradient based algorithm could not be used.

Although the ranges of design variables were limited in order to avoid geometries that would not converge in MSES (clashing flap and main element, too large a gap, sharp flap leading edge etc.), a lot of randomly chosen designs within the lower and upper bounds of design variables still produced problematic geometries. Because of this problem, only one generation of genetic algorithm with population size of 1000 was run at the beginning to obtain a sufficient number of feasible designs. Best 100 designs were selected and used as an initial population for the second stage genetic algorithm.

Three angles of attack were analysed in each iteration. On average, MSES took about 10 seconds to perform a single angle of attack calculation. As the optimization was run on an 8 core processor, 8 runs were run in parallel. Because of difficulties with convergence, all 8 parallel runs were run at the same angle of attack but with different mesh sizes, some of which had to converge for successful designs. It is then a question of how many different mesh sizes are tried before the design is discarded that heavily impacts the computation time. Many different strategies were tried during the process. Typical optimization took less then 2 days to finish on an 8 core processor.

3 Analysis and Design

Besides the general objective of maximizing the maximum lift coefficient of the two element airfoil configuration, separation should be prevented at all angles of attack. Separated flow over the flap at low angles of attack is a common problem in two element airfoil design because an optimally designed flap for maximum lift experiences high suction peak at its leading edge when there is not enough circulation on the main element to suppress it [17]. To keep the optimization process within feasible time constraints, it was not possible to evaluate each design over the entire angle of attack range. Finding the right criteria to ensure that the optimized design does not experience separation at the angles of attack that could not be analyzed within the optimization loop was one of the major problems of the project.

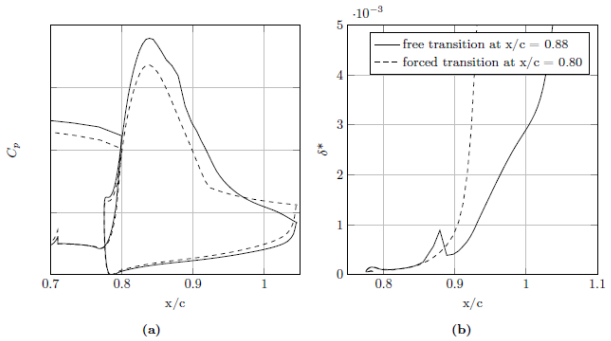

Fig. 5: Pressure distributions (a) and boundary layer displacement thickness on the flap upper surface (b) for the same design with free and forced transition location (Re = 2.1e6)

After running the MSES calculations with free transition, it emerged that the majority of promising designs developed laminar separation bubbles and turbulent reattachment on the upper surface of the flap. When the same design was analyzed with a forced transition in front of the pressure recovery region, the turbulent boundary layer would separate at the chordwise location where in free transition case it only transitioned from laminar to turbulent. Displacement thickness over the flap for both cases is shown in figure 5. Since turbulent boundary layer should be able to resist higher adverse pressure gradients before separation than laminar [14], it is questionable whether the free transition case is realistic. For all the following optimization runs it was decided to trip the boundary layer on the flap before it reaches the suction peak, as this case represented less margin to separation for MSES. Additional two reasons for forcing the transition were a) that the actual transition location may well be at the earlier point than what MSES predicts due to turbulence in the vicinity of the main element cove where the flow is separated and b) because in case of hysteresis being observed during wind tunnel testing of the final design, a zigzag tape might be fitted to the flap leading edge to force early transition [5].
In order to ensure attached flow over an entire angle of attack range, the generated geometries were evaluated with MSES at three diff erent angles of attack: -5, 8 and 12 . Initially, the objective function was formulated with equation (7). $a_{-5,8}$ stands for lift curve slope between angles of attack of -5 and 8 . If the slope was higher than 2π, which happened if the flow was separated at -5 and attached at 8, the *K*-factor was set to a finite number, thus representing a penalty to the objective function that increased with increasing lift slope increment. If the slope was lower than 2π, *K* was set to 0.

$$f_{obj} = -\left(W_{payload} - K\left(a_{-5,8} - 2\pi\right)\right) \qquad (7)$$

This approach was not successful since the optimized design had separated flow at both -5 and 8 degrees, thus giving a lift slope not higher than 2π. Reattachment happened between 8 and 12 degrees angle of attack, giving high maximum C_L.
Changing the range at which the slope was computed was impractical since at higher angles of attack the slope would be much lower than 2 even for optimized designs due to wake bursting. Therefore no practical criteria could be found to control the separation through lift curve slope while keeping the number of angles of attack to compute at three.
Another solution was then implemented in which the displacement thickness of the boundary layer on the flap upper surface was output from MSES calculation for each case. If the maximum displacement thickness, as defined in figure 6 as δ^*_{max}, was higher than the prescribed limit for any of the analyzed angles of attack, the optimizer would discard the design. To find the appropriate value of displacement thickness limit, local optimizations were run with diff erent values. The results are shown in figure 7. $\delta^*_{max} = 0.02$ was chosen as the limit for further optimization runs since the curve in figure 7 corresponding to this value has highest CL max2D of all curves that do not have any increase in lift curve slope throughout the whole angle of attack range.

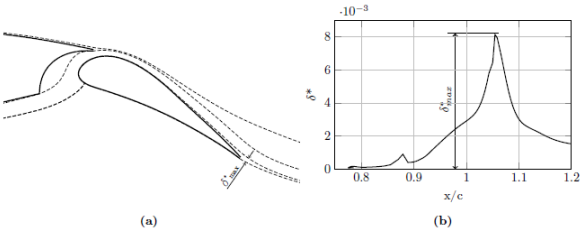

Fig. 6: Maximum displacement thickness max of the flap wake.

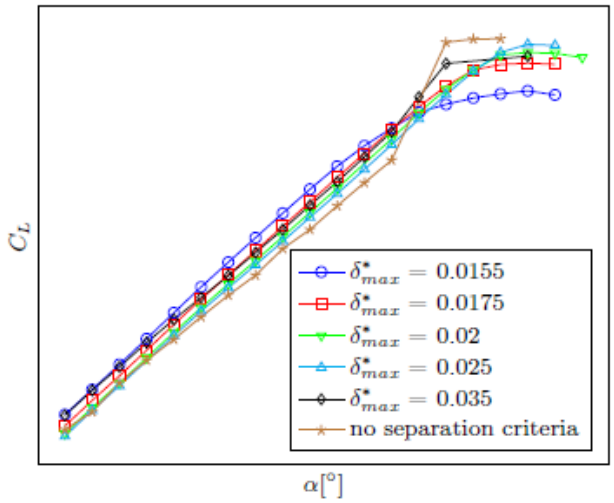

Fig. 7: Lift curves of locally optimized designs for diff erent max limits.

4 Results and Discussion

Four diff erent optimization runs are discussed, diff ering by slight changes in design space and constraints, as shown in table 1. The runs are referred to by names indicating the date of running (*Jun10*, *Jun12*, *Jun13* and *Jun15*).

Table 1: Design space for four optimizations; only changes w.r.t. preceding design are indicated.

Variable	*Jun10*	*Jun12*	*Jun13*	*Jun15*
C_1 C_2	[0.12 0.15]			
C_2	[0.72 0.75]		[0.74 0.77]	
dR_1	[0.00 0.60]			
t_2	[0.03 0.08]			
C_{3Y1}	[-0.03 0.02]			[-0.03 0.01]
C_{3dY2}	[0.005 0.05]			[0.005 0.04]
HP_Y	[-0.30 -0.14]	[-0.16 -0.14]		
dHP_X	[0.00 0.03]			
δ_f	[20.0 30]			
C_{3X}	0.70		0.72	
flap l.e. limit	no explicit limit		0.71	0.72

Before the final results (table 2), first some general observations are discussed.
Figure 8 plots payload w.r.t. $C_{l,max2D}$ for all the designs during an exemplary optimization run. It can be seen that payload depends predominantly on $C_{l,max2D}$. For the same $C_{l,max2D}$ there is not much variation in payload between diff erent flap designs that achieve the same $C_{l,max2D}$: about 10 kg for lift coefficients of about 2.4 and only about 2 kg for the highest lift coefficients. This indicates that when the design is selected down to the type of the high lift

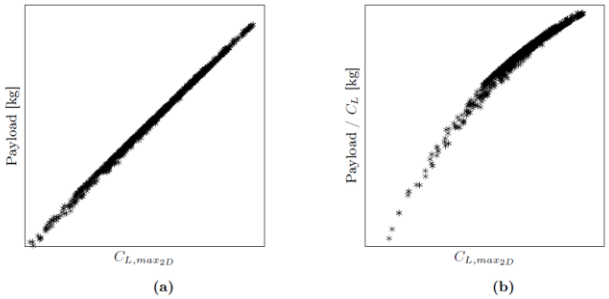

Fig. 8: Payload with respect to CL;max2D for all iterations of an exemplary optimization.

system and constrained with clean configuration and spanwise position, the optimization process is more an aerodynamic optimization than a highly coupled multidisciplinary optimization. The method of limiting the maximum displacement thickness of the flap wake (as described in section 3) proved to be very reliable since all the optimized designs showed no signs of separation when they were analyzed over the whole angle of attack range after the optimization finished.
The limiting factor in determining the maximum lift was not flow separation off the airfoil surface, but rather the bursting of main element's wake. As shown in figure 12, the wake of the main element widens extremely when it is close enough to the flap surface and therefore the positive pressure gradient at the flap surface is imposed on it [14]. A wide wake can be seen as a large displacement body that prevents the flow from following the flap surface, causing a decambering eff ect and thus reducing the lift. Minimizing wake bursting turned out to be the key to achieving high lift coefficients. Amount of wake bursting is mainly determined by at the main element's trailing edge and the positive pressure gradient on the flap upper surface. Since the main element geometry cannot be changed, there is not much that can be done about the as it is mainly determined by the pressure recovery region from the flap leading edge towards the trailing edge. Pressure gradient on the flap will as well have to be on the limit of separation if the

Table 2: Optimization results for designs from table 1 (subscript plain denotes the value with plain flap design).

Variable	*Jun10*	*Jun12*	*Jun13*	*Jun15*
$CL\ max_{2D}$ / $CL\ max_{2D,plain}$ [-]	1.26	1.26	1.27	1.21
$CL\ max_{3D}$ / $CL\ max_{3D,plain}$ [-]	1.125	1.125	1.13	1.10
$Payload$ / $Payload_{plain}$ [-]	1.39	1.41	1.42	1.33
$MTOM$ / $MTOM_{plain}$ [-]	1.125	1.125	1.130	1.100
$W_{payload}$ / $MTOW$ [-]	0.818	0.839	0.842	0.864
HP_Y [-]	-0.298	-0.157	-0.150	-0.151
$C_{D\ fairings}$ [-]	0.0018	0.0010	0.0010	0.0010
$M_{fuel\ fairing}$ [-]	0.053	0.030	0.030	0.030
$Flapl\ e.x.-\ coord$ [-]	0.702	0.692	0.718	0.721
$(C1_X - C2_X)_{eff}$ [-]	0.110	0.075	0.065	0.079
gap [-]	0.029	0.021	0.02	0.02
$overlap$ [-]	0.010	0.033	0.025	0.031
$\delta_{f\ landing}$ [o]	24.5	23.6	24.7	25.5
$\delta_{f\ TO}$ [o]	15.5	14.6	16.7	14.5
$(L/D)_{@MTOW0}$ / $(L/D)_{@MTOW0\ plain}$ []	1.033	1.038	1.029	1.039
$\gamma_{@MTOW0}$ / $\gamma_{@MTOW0\ plain}$ [-]	1.031	1.046	1.031	1.046
s_{TO} / $s_{TO\ plain}$ [-]	1.119	1.122	1.126	1.094
$s_{landing}$ / $s_{landing\ plain}$ [-]	1.160	1.161	1.165	1.142

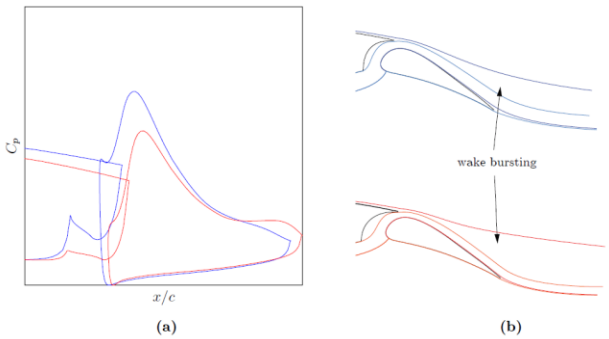

Fig. 9: Effect of flap position on wake bursting

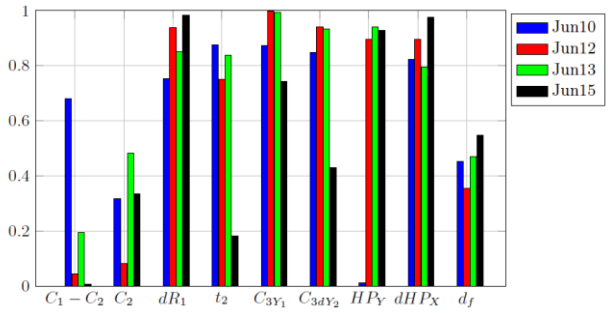

Fig. 10: Design parameters for optimized designs, nondim. w.r.t. Jun10 optimization design space.

configuration is to carry a maximum amount of lift. The most effective way of minimizing wake bursting was to position the flap further away from the main element's wake in order to reduce the pressure gradient experienced by the wake, while still maintaining small enough gap that maximizes the circulation effect of the two elements on each other. This effect can be seen in figure 9. The downward shift of the flap at constant *f* is achieved with a forward shift of the hinge point, dHP_X. All the optimized designs have a relatively high value of this parameter, as seen in figure 10.

From results in table 2, it is observed that, at least for *Jun10*, *Jun12* and *Jun13* cases, slight changes in initial design space return considerably different designs, but obtain similar values of payload. It can also be seen that the optimization does not return a true global minimum, since the final *Jun12* design gives slightly higher payload than the *Jun10*, but is also feasible under *Jun10* design space. *Jun10* design space allows for very deep hinge point location that is in general favorable in achieving high lift coefficients, but also has higher drag in cruise condition.
Indeed the *Jun10* design needs about 2% of fuel more than the *Jun13* design for the same range

of 1000 nm. For the *Jun12*, *Jun13* and *Jun15* optimizations, the hinge point location was limited between -0.14c and -0.16c, because it was felt that similar lift coefficients are possible with higher hinge positions, which was proven by *Jun12* and *Jun13* designs. The downside of the *Jun12* design is the most forward point of the flap in clean configuration at 0.692c, which would need a slight forward shift of the rear spar. For *Jun13* and *Jun15* cases, the flap leading edge position was limited definitely, not only with the x-coordinate of the b-spline control points. This did not prove to be problematic in terms of high lift, since the *Jun13* design even has a marginally higher lift than the *Jun12* design. Because the *Jun13* design has the lowest eff ective distance between lower and upper flap breaks ($(C1_X - C2_X)_{eff}$), this resulted in the worst take-off performance of all designs (see table 2), because a short $(C1_X - C2_X)_{eff}$ generally allows lower range of usable flap deflections. Table 2 shows that the diff erence between landing and take-off flap deflection angle is 1 less for the *Jun13* design than for the others. That is why another optimization was run, the *Jun15*, which had more limits on the b-spline control points location which increased the $(C1_X - C2_X)_{eff}$ by 20% w.r.t. the *Jun13* case, but was the only design that had considerably lower maximum lift coefficient and payload. Realizing that the take-off performance deficit of the *Jun13* result is small, the author feels that this design is the most suitable for implementation on the aircraft.

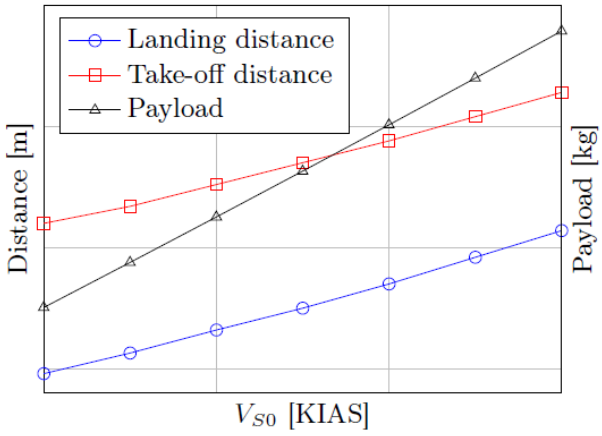

Fig. 11: Payload and field length dependency on stall speed V_{S0}.

The take-off and landing distance increase considerably when the *MTOW* is increased due to new high lift system while the stall speed V_{S0} is kept constant. It is possible to sacrifice some of the *MTOW* (and payload) with decreasing the V_{S0} to decrease the field length, as shown in figure 11. This analysis takes into account the decrease in weights of fuel, wing and landing gear as a function of *MTOW*.

5 Conclusions and recommendations

Multidisciplinary optimization of a high lift system with a single slotted flap on a propeller driven general aviation aircraft showed the following conclusions:

- A simple dropped hinge mechanism can be used to achieve sufficient high lift performance to increase the maximum lift coefficient of the aircraft by 12% with respect to a plain flap high lift system.
- If the stall speed is kept constant, the *MTOW* increases by 13% and the payload increases by 40%. Take-off distance increases by 12.5% and landing distance by 17.5%, but can be traded off with increase in payload if the stall speed is decreased.
- The additional cruise drag due to hinge fairings increases the fuel weight for the range of 1000 nm by 3% for a hinge position of 0.15c below the chord line and three supports per flap.
- Limiting phenomena in determining the highest lift coefficient is the bursting of main element's wake, rather than flow separation off the surface.
- When it is not feasible to compute the whole angle of attack range in each iteration during an optimization, three angles of attack are enough to avoid jumps in the lift curve if a limit on boundary layer displacement thickness at the flap trailing edge is used as a constraint.

Asking the original research question, what is the optimal high lift system design for a highly efficient 4-seater general aviation aircraft for improved payload, it can be concluded that a single slotted flap with a simple dropped hinge is the best compromise between complexity and performance for such an application.

For further research on the current theme, the following recommendations can be made:

- The model for prediction of fairing drag might be underpredicting the actual drag, therefore a CFD simulation of such fairings in combination with the wing should be performed for validation.
- The present optimization scheme would only need a minor extension to allow the analysis of more complex flap mechanisms such as a four bar linkage. This could be implemented in future to analyze the benefits of such a system, if a designer is willing to implement a more complex solution.
- It should be investigated why the MSES convergence is dependent on slight changes in mesh size for the same case, while the meshes that do converge give almost identical results. If convergence on any mesh size (within a certain range) could be achieved, the computation time could be reduced by a factor of about 4.

References

[1] Federal Aviation Regulations, Part 23. Federal Aviation Administration, 2014.

[2] I.H. Abbot and H. Greenberg. Tests in the variable density wind tunnel of the NACA 23013 airfoil with plain and split flaps. Technical Report NACA Report 661, NACA, 1939.

[3] Anon. Maximum lift of with trailing-edge flaps at low speeds. Technical report, ESDU.

[4] Anon. Wing lift coefficient increment at zero angle of attack due to deployment of single-slotted flaps at low speeds. Technical report, ESDU.

[5] M. Baragona, L.M.M. Boermans, M.J.L. van Tooren, H. Bijl, and A. Beukers. Bubble bursting and stall hysteresis on single-slotted flap high-lift configuration. AIAA Journal, 41(7):1230–1237, 2003.

[6] F.G.A. Bertels. Design framework for flap system kinematics, a knowledge based engineering application. Master's thesis, TU Delft, Faculty of aerospace engineering, 2012.

[7] Jones F. Cahill. Summary of section data on trailing-edge high-lift devices. Technical Report NACA Report 938, NACA, 1949.

[8] Mark Drela. Newton solution of coupled viscous/inviscid multielement airfoil flows. AIAA 21st Fluid Dynamics, Plasma Dynamics and Lasers Conference, Seattle, WA, U.S.A, June 1990. AIAA.

[9] Snorri Gudmundsson. General aviation aircraft design. Butterworth-Heinemann, 2013.

[10] Sighard F. Hoerner. Fluid-dynamic drag. Hoerner Fluid Dynamics, 1965.

[11] Daniel P. Raymer. Aircraft Design: A Conceptual Approach. AIAA Education Series, 5th edition, 2012.

[12] J. Roskam. New airfoils and higher wing loadings: a new look at general aviation airplane design. TU Delft, 1974.

[13] SKF. Linear actuators product range. accessed 11th June 2015.

[14] A.M.O. Smith. High-lift aerodynamics. AIAA Journal, 12(6):501–530, 1975.

[15] E. Torenbeek. Synthesis of subsonic airplane design. Delft university press, 1982.

[16] E. Torenbeek. Development and application of a comprehensive, design sensitive weight prediction method for wing structures of transport category aircraft, 1992.

[17] J. Wild. Mach and reynolds number dependencies of the stall behaviour of high-lift wing-sections. AIAA Journal, 50(4):1202–1216, 2013.

[18] A.D. Young. The induced drag of flapped elliptic wings with cut-out and with flaps that extend the local chord. Technical report, Aeronautical Research Council.

Contact Author Email Address

d.steenhuizen@tudelft.nl

Copyright Statement